Control of Photoinduced Energy- and Electron-Transfer Steps in Zinc Porphyrin−Oligothiophene−Fullerene Linked Triads with Solvent Polarity

Takumi Nakamura,[†] Jun-ya Ikemoto,[‡] Mamoru Fujitsuka,[†,§] Yasuyuki Araki,[†] Osamu Ito,*[,†] Kazuo Takimiya,[‡] Yoshio Aso,[‡,§] and Tetsuo Otsubo*[,‡]

Institute of Multidisciplinary Research for Advanced Materials, Tohoku University, CREST (JST), Katahira, Sendai, Miyagi 980-8577, Japan, and Department of Applied Chemistry, Graduate School of Engineering, Hiroshima University, Higashi-Hiroshima 739-8527, Japan

Received: December 14, 2004; In Final Form: March 25, 2005

The dramatic changes of the lifetimes of the charge-separated (CS) states were confirmed in zinc porphyrin (ZnP)−oligothiophene (*n*T)−fullerene (C_{60}) linked triads (ZnP−*n*T−C_{60}) with the solvent polarity. After the selective excitation of the ZnP moiety of ZnP−*n*T−C_{60}, an energy transfer took place from the ^{1}ZnP* moiety to the C_{60} moiety, generating ZnP−*n*T−$^1C_{60}$*. In polar solvents, the CS process also took place directly via the ^{1}ZnP* moiety, generating ZnP$^{\bullet+}$−*n*T−$C_{60}^{\bullet-}$, as well as the energy transfer to the C_{60} moiety. After this energy transfer, an indirect CS process took place from the $^1C_{60}$* moiety. In the less polar solvent anisole, the radical cation (hole) of ZnP$^{\bullet+}$−*n*T−$C_{60}^{\bullet-}$ shifted to the *n*T moiety; thus, the *n*T moiety behaves as a cation trapper, and the rates of the hole shift were evaluated to be in the order of 10^8 s^{-1}; then, the final CS states ZnP−*n*T$^{\bullet+}$−$C_{60}^{\bullet-}$ were lasting for 6−7 μs. In the medium polar solvent *o*-dichlorobenzene (*o*-DCB), ZnP−*n*T$^{\bullet+}$−$C_{60}^{\bullet-}$ and ZnP$^{\bullet+}$−*n*T−$C_{60}^{\bullet-}$ were present as an equilibrium, because both states have almost the same thermodynamic stability. This equilibrium resulted in quite long lifetimes of the CS states (450−910 μs) in *o*-DCB. In the more polar benzonitrile, the generation of ZnP−*n*T$^{\bullet+}$−$C_{60}^{\bullet-}$ was confirmed with apparent short lifetimes (0.6−0.8 μs), which can be explained by the fast hole shift to more stable ZnP$^{\bullet+}$−*n*T−$C_{60}^{\bullet-}$ followed by the faster charge recombination. It was revealed that the relation between the energy levels of two CS states, which strongly depend on the solvent polarity, causes dramatic changes of the lifetimes of the CS states in ZnP−*n*T−C_{60}; that is, the most appropriate solvents for the long-lived CS state are intermediately polar solvents such as *o*-DCB. Compared with our previous data for H_2P−*n*T−C_{60}, in which H_2P is free-base porphyrin, the lifetimes of the CS states of ZnP−*n*T−C_{60} are ∼30 times longer than those in *o*-DCB.

Introduction

Photoinduced electron transfer is one of the most interesting research fields attracting much attention. An electron-transfer rate is mainly governed by factors such as the redox potentials (E_{redox}) of the electron acceptor and donor, the reorganization energy (λ), the electronic coupling (V), and the distance between the acceptor and donor moieties (R(D−A)).[1−10] According to the Marcus theory, a charge-separated (CS) state lives for a longer time when the charge-recombination (CR) process occurs at the deep position in the inverted region.[11] Taking these points into consideration, many research groups have designed intramolecular electron-transfer systems for long-lived CS states. Because fullerene (C_{60}) has unique characteristics such as a low reduction potential (E_{red}) and a small λ value,[12−15] many research groups have reported the photophysical and photochemical properties of fullerene−donor linked dyad molecules.[16] A lot of groups have designed intramolecular multistep electron-transfer systems using various donors and acceptors.[9,17−21] In the previous study, we synthesized triads with free-base porphyrin (H_2P), oligothiophenes (*n*T), and C_{60}, which were abbreviated as H_2P−*n*T−C_{60} in our previous paper.[22a,b] In H_2P−*n*T−C_{60}, the H_2P moiety acts as an antenna and an electron donor, the *n*T moiety acts as a linker, and the C_{60} moiety acts as an electron acceptor. In H_2P−*n*T−C_{60} triads, the fluorescence of the H_2P moiety was quenched by introduction of the C_{60} moiety, comparing with H_2P−*n*T dyads,[22a,b] which suggests the direct generation of CS states ($H_2P^{\bullet+}$−*n*T−$C_{60}^{\bullet-}$) from $^1H_2$P*−*n*T−C_{60}; after hole shift (HS) from $H_2P^{\bullet+}$−*n*T−$C_{60}^{\bullet-}$, H_2P−*n*T$^{\bullet+}$−$C_{60}^{\bullet-}$ was confirmed as the final CS state with lifetimes shorter than 20 μs in polar solvents such as benzonitrile (PhCN) and *o*-dichlorobenzene (*o*-DCB).[22a] To maintain the CS states for a longer time, it is necessary to use the porphyrin moiety (Por) having a lower oxidation potential (E_{ox}) than the *n*T moiety. Then, it is expected that the relative stability (ΔG_{RIP}) of two CS states such as Por−*n*T$^{\bullet+}$−$C_{60}^{\bullet-}$ and Por$^{\bullet+}$−*n*T−$C_{60}^{\bullet-}$ is changeable by solvent polarity, because the energies of these CS states strongly depend on the distance between the donor and the acceptor and their radii, as suggested by Weller's equation.[23,24] Hence, considering the oxidation potential (E_{ox}), the zinc porphyrin (ZnP) must be more proper for the terminal electron donor than H_2P (Figure 1), because three cases of the relative stability (ΔG_{RIP}) of ZnP−*n*T$^{\bullet+}$−$C_{60}^{\bullet-}$ and ZnP$^{\bullet+}$−*n*T−$C_{60}^{\bullet-}$ are possible by changing the solvent polarity: ΔG_{RIP}(ZnP−*n*T$^{\bullet+}$−$C_{60}^{\bullet-}$) < ΔG_{RIP}(ZnP$^{\bullet+}$−*n*T−$C_{60}^{\bullet-}$), ΔG_{RIP}(ZnP−*n*T$^{\bullet+}$−$C_{60}^{\bullet-}$) = ΔG_{RIP}(ZnP$^{\bullet+}$−*n*T−$C_{60}^{\bullet-}$), and ΔG_{RIP}(ZnP−*n*T$^{\bullet+}$−$C_{60}^{\bullet-}$) > ΔG_{RIP}(ZnP$^{\bullet+}$−*n*T−$C_{60}^{\bullet-}$) in less, medium, and more polar solvents, respectively. In the present study, we examined the CS and CR processes as well as the energy-

* To whom correspondence should be addressed. E-mail: ito@tagen.tohoku.ac.jp (O.I.); otsubo@hiroshima-u.ac.jp (T.O.).
† Tohoku University.
‡ Hiroshima University.
§ Present address: The Institute of Scientific and Industrial Research, Osaka University, Ibaraki, Osaka 567-0047, Japan.

10.1021/jp044316v CCC: $30.25
Published on Web 07/12/2005

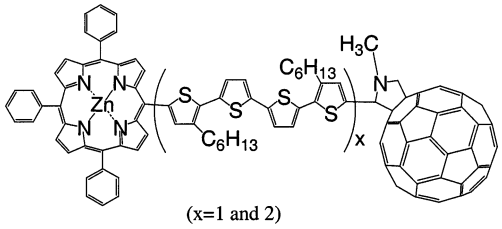

Figure 1. Molecular structures of ZnP−*n*T−C_{60}.

transfer (EN) process in ZnP−*n*T−C_{60} by time-resolved absorption and fluorescence measurements in four solvents—toluene, anisole, *o*-DCB, and PhCN. In the last three polar solvents, the CS processes are expected to occur when the ZnP moiety is photoexcited. Especially in *o*-DCB, the energy of $ZnP^{\bullet+}$−*n*T−$C_{60}^{\bullet-}$ is equal to that of ZnP−$nT^{\bullet+}$−$C_{60}^{\bullet-}$, which is produced via the HS process or the indirect CS process via ZnP−*n*T−$^1C_{60}$*. Our main goal of the present study is to maintain the CS states for a long time by controlling the driving force for the CR process by changing the solvent polarity. In addition, to investigate the distance dependence of the efficiencies of the CS and EN processes, we compared two triads including different *n*T (*n* = 4 and 8), which are expected to act as a molecular wire and as a positive charge trapper (=electron donor) with respect to $ZnP^{\bullet+}$. It is well understood that the E_{ox} values of *n*T decrease with their lengths, because the π-conjugation extends along the *n*T chain.[25] These triads including the ZnP moiety are expected to absorb visible light more efficiently than the *n*T−C_{60} dyads; thus, the photoinduced processes with high light harvesting ability initiated by the excitation of the ZnP moiety have been investigated in the present study.

Experimental Section

Materials. Syntheses of ZnP−*n*T−C_{60} were performed by the insertion of the Zn atom into the corresponding H_2P−*n*T−C_{60},[22b] with refluxing them in the presence of $Zn(OAc)_2$. Components such as *n*T (*n* = 4 and 8) and *N*-methylpyrrolidino-C_{60} ($NMPC_{60}$) were prepared according to the methods described in the literature.[22b] Other chemicals such as zinc tetraphenylporphyrin (ZnTPP) and the solvents (anisole, benzonitrile (PhCN), *o*-dichlorobenzene (*o*-DCB), and toluene) were of the best commercial grade available.

General. All chemicals are of reagent grade. The melting points are uncorrected. ^{1}H NMR spectra were measured on a JEOL Lambda 400 spectrometer using deuteriochloroform or deuteriodimethyl sulfoxide as solvent and tetramethylsilane as internal standard. MS spectra were recorded on a Shimadzu KOMPACT-MALDI PROBE spectrometer using a dithranol matrix.

ZnP−4T−C_{60} and ZnP−8T−C_{60}. A typical experimental procedure is described for the synthesis of ZnP−4T−C_{60} as follows: A solution of H_2P−4T−C_{60} (31.4 mg, 0.017 mmol) in chloroform (5 mL) was mixed with a solution of zinc acetate (26.6 mg, 0.12 mmol) in methanol (2 mL). The mixture was refluxed for 1 h in a nitrogen atmosphere and washed with water (10 mL × 3). After dryness over anhydrous sodium sulfate, the organic layer was directly subjected to column chromatography on alumina with 1:1 hexane−dichloromethane as an eluent to give a brown powder of ZnP−4T−C_{60} (23.7 mg).

ZnP−4T−C_{60}. Yield 71% from H_2P−4T−C_{60}; mp 265 °C (decomp); ^{1}H NMR (400 MHz, $CDCl_3$) δ 9.30 (d, *J* = 4.88 Hz, 2H), 8.94 (d, *J* = 4.88 Hz, 2H), 8.91 (s, 4H), 8.16−8.20 (m, 6H), 7.73−7.75 (m, 9H), 7.75 (s, 1H), 7.24 (d, *J* = 3.78 Hz, 1H), 7.16 (d, *J* = 3.78 Hz, 1H), 7.12 (d, *J* = 3.80 Hz, 1H), 7.05 (s, 1H), 7.00 (d, *J* = 3.80 Hz, 1H), 4.77 (s, 1H), 4.53 (d, *J* = 9.64 Hz, 1H), 3.73 (d, *J* = 9.64 Hz, 1H), 3.09 (t, *J* = 7.82, 2H), 2.82 (s, 3H), 2.74 (t, *J* = 7.82 Hz, 2H), 1.90−1.97 (m, 2H), 1.53−1.62 (m, 2H), 1.19−1.47 (m, 12H), 0.79−0.92 (m, 6H); MS(MALDI-TOF) *m*/*z* 1873.9 (M^+, calcd 1873.3).

ZnP−8T−C_{60}. Yield 68% from H_2P−8T−C_{60}; brown powder; mp 195 °C (decomp); ^{1}H NMR (400 MHz, $CDCl_3$) δ 9.33 (d, *J* = 4.88 Hz, 2H), 8.97 (d, *J* = 4.88 Hz, 2H), 8.91 (s, 4H), 8.18−8.21 (m, 6H), 7.74−7.78 (m, 9H), 7.75 (s, 1H), 7.28 (d, *J* = 3.90 Hz, 1H), 7.21 (d, *J* = 3.90 Hz, 1H), 7.16 (d, *J* = 3.88 Hz, 1H), 7.13 (s, 1H), 7.07 (d, *J* = 3.78 Hz, 2H), 7.03 (d, *J* = 3.88 Hz, 1H), 6.99 (d, *J* = 3.78 Hz, 2H), 6.97 (s, 2H), 4.95 (s,1H), 4.73 (d, *J* = 9.76 Hz, 1H), 3.95 (d, *J* = 9.76 Hz, 1H), 3.13 (t, *J* = 7.82 Hz, 2H), 2.89 (s, 3H), 2.70−2.77 (m, 6H), 1.94−1.99 (m, 2H), 1.59−1.68 (m, 6H), 1.21−1.44 (m, 24H), 0.80−0.95 (m, 12H); MS(MALDI-TOF) *m*/*z* 2371.6 (M^+, calcd 2371.5).

Methods. Molecular orbital calculations were performed using density functional theory (DFT) at the B3LYP/3-21G(*) level.[26]

Square wave volumetric measurements were carried out with a potentiostat (BAS CV50W) and a cell equipped with a platinum working electrode, an Ag/Ag^+ reference electrode, and a platinum counter electrode. All electrochemical measurements were performed in anisole, *o*-DCB, and PhCN containing 0.10 M tetra-*n*-butylammonium hexafluorophosphate ($(n\text{-}C_4H_9)_4NPF_6$, Nacalai Tesque) at room temperature. The redox potentials (E_{redox}) were corrected against the ferrocene/ferrocenium (Fc/Fc^+) couple.

Steady-state absorption spectra were measured on a JASCO V-530 UV−vis spectrophotometer. Steady-state fluorescence spectra were measured on a Shimadzu RF-5300 PC spectrofluorophotometer.

The fluorescence lifetimes were measured by a single-photon counting method with a streak scope (Hamamatsu Photonics, C4334-01) using the second harmonic generation (SHG, 400 nm) of a Ti:sapphire laser (Spectra-Physics, Tsunami 3950-L2S, fwhm 150 fs) as an excitation source.

The picosecond transient absorption spectra were measured by the pump and probe method using a Ti:sapphire regenerative amplifier seeded by the SHG of an Er-doped fiber laser (Clark-MXR CPA-2001 plus, 1 kHz, fwhm 150 fs). A white continuum pulse used as a monitoring light was generated by focusing the fundamental of the amplifier on a rotating H_2O cell. The samples were excited by the SHG (388 nm) of fundamental or output of OPA (Clark-MXR vis-OPA, 560 nm). The monitoring light transmitted through the sample in a rotating cell was detected with a dual MOS detector (Hamamatsu Photonics, C6140) equipped with a polychromator for the visible region or an InGaAs linear image sensor (Hamamatsu Photonics, C5890-128) for the near-IR region.

The nanosecond transient absorption spectra were measured using the pulsed laser light from an optical parametric oscillation (Continuum Surelite OPO, fwhm 4 ns) pumped by a Nd:YAG laser (Continuum, Surelite II-10). For the measurements of the transient absorption spectra in the near-IR region for a time scale shorter than 5 μs, a Ge avalanche photodiode (APD, Hamamatsu Photonics, B2834) was used as a detector for monitoring light from the pulsed xenon lamp. For a time scale longer than 5 μs, an InGaAs photodiode was used as a detector for monitoring light from the continuous xenon lamp.

Results and Dscussion.

Steady-State Absorption Spectra. Absorption spectra of ZnP−4T−C_{60} and the components ZnTPP, 4T, and $NMPC_{60}$ in PhCN are shown in Figure 2a. The B-band of the ZnP moiety

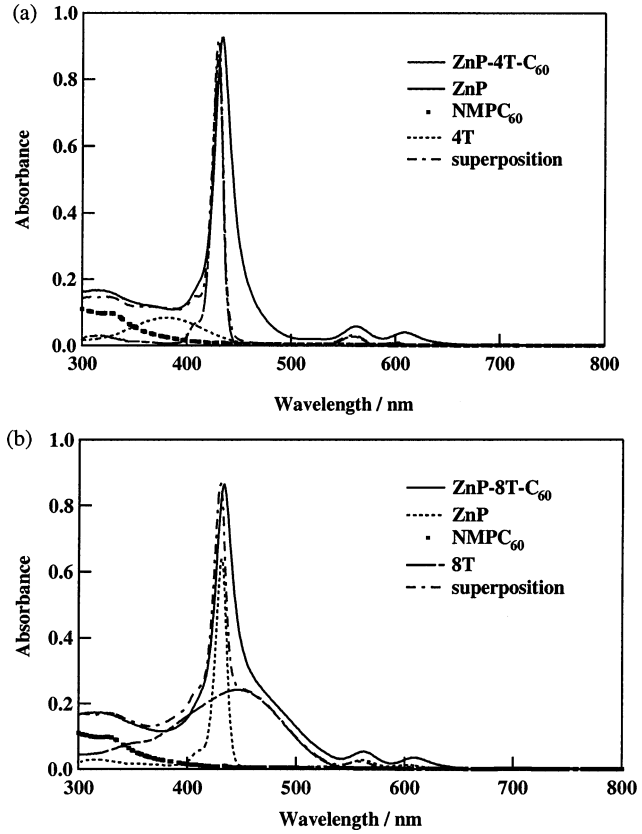

Figure 2. Steady-state absorption spectra of (a) ZnP−4T−C_{60} and (b) ZnP−8T−C_{60} in PhCN.

in ZnP−nT−C_{60} shifted slightly to a longer wavelength and became broader than that of ZnTPP. Similar absorption spectra were observed for ZnP−8T−C_{60}, as shown in Figure 2b. These findings suggest that the symmetry of the ZnP moiety in ZnP−*n*T−C_{60} becomes lower than the highly symmetric ZnTPP, but appreciable interaction between the ZnP moiety and the *n*T moiety in ZnP−*n*T−C_{60} may not be present.

One-Electron Redox Potentials and ET Driving Force. The E_{ox} and E_{red} values of ZnP−*n*T−C_{60} were evaluated by square wave voltammetry in anisole, *o*-DCB, and PhCN, as summarized in Table 1. The E_{ox} values shifted progressively to a more negative direction as the solvent polarity was increased: anisole ($\epsilon_S = 4.33$) < *o*-DCB ($\epsilon_S = 9.93$) < PhCN ($\epsilon_S = 25.2$),[27] where ϵ_S refers to the solvent dielectric constant. Negative shifts in oxidation potentials are principally rationalized by a stronger solvation of the resulting radical cations of the ZnP and *n*T moieties in polar solvents. On the other hand, the reduction potentials shifted to a positive direction in polar solvents, which was due to solvation of the radical anion in polar solvents.

The E_{ox} values of the ZnP moieties are lower than those of the *n*T moieties in the dyads and triads. Therefore, the ZnP moiety mainly works as an electron donor. Because the E_{ox} value of the 4T moiety is similar to that of the 8T moiety in the dyads and triads, the differences in kinetic data (vide infra) must be attributed to the length of the *n*T moiety rather than the electronic factors. From the E_{red} values, the order of the electron-acceptor abilities is ZnP < *n*T ≪ C_{60}.

The free-energy changes for the CS and CR processes ($-\Delta G_{CS}$ and $-\Delta G_{CR}$) were calculated by Weller's eqs 1 and 2;[23]

$$-\Delta G_{CR} = E_{ox} - E_{red} - e^2/(\epsilon_S R(\mathrm{D-A})) \quad (1)$$

$$-\Delta G_{CS} = \Delta E_{0-0} - (-\Delta G_{CR}) \quad (2)$$

where R(D−A) refers to the center-to-center distance between the donor and the acceptor and ΔE_{0-0} refers to the energies of the ^{1}ZnP* and $^1C_{60}$* moieties.

To obtain insight into the optimized structures of ZnP−*n*T−C_{60}, computational studies were performed using density functional theory (DFT) at the B3LYP/3-21G(*) level (Supporting Information Figures S1 and S2).[26] From the DFT-optimized structures of ZnP−4T−C_{60} and ZnP−8T−C_{60}, the R(D−A) values were determined as follows: R(ZnP−C_{60}) = 25.3 Å, R(4T−C_{60}) = 12.8 Å, and R(ZnP−4T) = 12.5 Å for ZnP−4T−C_{60} and R(ZnP−C_{60}) = 40.5 Å, R(8T−C_{60}) = 20.4 Å, and R(ZnP−8T) = 20.1 Å for ZnP−8T−C_{60}, respectively. According to eqs 1 and 2, the driving force for the CS process is governed by ϵ_S; therefore, the driving force can be controlled by changing the solvent. It is also notable that the energy levels of ZnP$^{\bullet+}$−8T−$C_{60}^{\bullet-}$ vary more widely than those of ZnP−8T$^{\bullet+}$−$C_{60}^{\bullet-}$ with the variation of the solvent polarity, because of the R(D−A) term in eq 1 (Supporting Information Figure S3). The ΔG_{CR} values are summarized in Table 2.

From these thermodynamic values and electronic transition energies, the energy diagram for ZnP−8T−C_{60} is illustrated in Figure 3. A similar energy diagram is obtained for ZnP−4T−C_{60}.

Steady-State Fluorescence Measurements. Figure 4 shows the fluorescence spectra of ZnP−4T−C_{60} and ZnP−4T obtained by excitation of the ZnP moiety with 420 nm light in PhCN and toluene, in which the sample concentrations were adjusted so that the same numbers of photons were absorbed by the ZnP moiety. The fluorescence band at 625 nm with a shoulder around 670 nm of ZnP−4T can be attributed to the ^{1}ZnP* moiety. Because the fluorescence intensity of ZnP−4T in PhCN was slightly weaker than that in toluene, a small amount of the CS process takes place between the ZnP and 4T moieties. From the negative ΔG_{CS} values (Supporting Information Table S1), both CS processes generating ZnP$^{\bullet-}$−4T$^{\bullet+}$ and ZnP$^{\bullet+}$−4T$^{\bullet-}$ via ^{1}ZnP*−4T are possible in PhCN. In toluene, the fluorescence intensity of the ^{1}ZnP* moiety of ZnP−4T−C_{60} decreased compared with that of ZnP−4T and a fluorescence peak of the $^1C_{60}$* moiety was confirmed around 700 nm (vide infra), suggesting the EN process to the C_{60} moiety in ZnP−4T−C_{60}. In PhCN, further decreases of the fluorescence intensities of the ^{1}ZnP* and $^1C_{60}$* moieties were observed compared with that in toluene, indicating the CS process to ZnP$^{\bullet+}$−4T−$C_{60}^{\bullet-}$ from ^{1}ZnP*−4T−C_{60} and to ZnP−4T$^{\bullet+}$−$C_{60}^{\bullet-}$ via ZnP−4T−$^1C_{60}$* after the EN process. These CS processes are supported by the negative ΔG_{CS} value in PhCN (−0.70 and −0.34 eV, respectively, from eq 2 using ΔG_{CR} in Table 2). In anisole and *o*-DCB, fluorescence quenching behavior similar to that in PhCN was observed, indicating that both CS processes and the EN process were included. For ZnP−8T and ZnP−8T−C_{60}, similar tendencies to ZnP−4T and ZnP−4T−C_{60} were observed in all solvents, respectively.

Fluorescence Lifetime Measurements in Toluene. Figure 5 shows the fluorescence temporal profiles of ZnP−8T and ZnP−8T−C_{60} after the excitation of the ZnP moiety in toluene and PhCN; for ZnP−4T and ZnP−4T−C_{60}, similar fluorescence temporal profiles to ZnP−8T and ZnP−8T−C_{60} were observed, respectively. The temporal profiles of ^{1}ZnP*−*n*T in toluene can be fitted with a single-exponential function, from which the fluorescence lifetime (τ_F) of the ^{1}ZnP* moiety was evaluated to be 1.2 ns. Because the τ_F values for ^{1}ZnP*−*n*T are independent from the *n*T moieties (Table 3), this value (1.2 ns) is a characteristic fluorescence lifetime (τ_0) of the ZnP moiety without the CS and EN processes in the dyads. τ_0^{-1} was defined

TABLE 1: Redox Potentials in Various Solvents

		E/V (vs $Fc/Fc^{\bullet+}$)[a]				
material	solvent	$ZnP/ZnP^{\bullet+}$	$nT/nT^{\bullet+}$	$C_{60}/C_{60}^{\bullet-}$	$ZnP/ZnP^{\bullet-}$	$nT/nT^{\bullet-}$
ZnP−4T	anisole	0.41	0.49		−1.70	−1.58
ZnP−4T−C_{60}	($\epsilon_S = 4.33$)	0.42	0.48	−1.18	−1.70	−1.60
ZnP−8T		0.39	0.48		−1.71	−1.55
ZnP−8T−C_{60}		0.40	0.49	−1.18	−1.72	−1.60
ZnP−4T	*o*-DCB	0.38	0.47		−1.70	−1.59
ZnP−4T−C_{60}	($\epsilon_S = 9.93$)	0.38	0.47	−1.13	−1.67	−1.57
ZnP−8T		0.36	0.46		−1.68	−1.53
ZnP−8T−C_{60}		0.37	0.46	−1.13	−1.68	−1.55
ZnP−4T	PhCN	0.31	0.46		−1.67	−1.54
ZnP−4T−C_{60}	($\epsilon_S = 25.2$)	0.32	0.46	−1.04	−1.63	−1.55
ZnP−8T		0.30	0.39		−1.60	−1.50
ZnP−8T−C_{60}		0.31	0.39	−1.04	−1.60	−1.51
$NMPC_{60}$				−1.04		

[a] An electrochemical cell equipped with a platinum working electrode, an Ag/Ag^+ reference electrode, and a Pt counter electrode. The electrolyte was 0.10 M $(n\text{-Bu})_4NPF_6$. The E_{redox} values were corrected against the Fc/Fc^+ couple.

TABLE 2: Driving Forces ($-\Delta G_{CR}$) of the CR Process of the CS States between ZnP and C_{60} or between *n*T and C_{60} in ZnP−*n*T−C_{60} in Toluene, Anisole, *o*-DCB, and PhCN

			$-\Delta G_{CR}$[a]/eV	
solvent	initial state	final state	$n = 4$	$n = 8$
toluene	$ZnP-nT^{\bullet+}-C_{60}^{\bullet-}$	ZnP−*n*T−C_{60}	1.83[b]	2.11[b]
	$ZnP^{\bullet+}-nT-C_{60}^{\bullet-}$	ZnP−*n*T−C_{60}	2.13[b]	2.38[b]
anisole	$ZnP-nT^{\bullet+}-C_{60}^{\bullet-}$	ZnP−*n*T−C_{60}	1.40	1.43
	$ZnP^{\bullet+}-nT-C_{60}^{\bullet-}$	ZnP−*n*T−C_{60}	1.48	1.50
o-DCB	$ZnP-nT^{\bullet+}-C_{60}^{\bullet-}$	ZnP−*n*T−C_{60}	1.46	1.49
	$ZnP^{\bullet+}-nT-C_{60}^{\bullet-}$	ZnP−*n*T−C_{60}	1.49	1.47
PhCN	$ZnP-nT^{\bullet+}-C_{60}^{\bullet-}$	ZnP−*n*T−C_{60}	1.45	1.42
	$ZnP^{\bullet+}-nT-C_{60}^{\bullet-}$	ZnP−*n*T−C_{60}	1.34	1.33

[a] From eq 1 except in toluene. [b] Estimated using $-\Delta G_{CR} = E_{ox} - E_{red} + (e^2/(4\pi\epsilon_0))[(1/(2R_+) + 1/(2R_-) - 1/R(D-A))/\epsilon_S - (1/(2R_+) + 1/(2R_-))/\epsilon_R]$, where R_+ and R_- are the radii of the cation and anion, respectively (4T, 7.5 Å; 8T, 14.5 Å; ZnP, 5.0 Å; $NMPC_{60}$, 4.2 Å). $R(D-A)$ is the center-to-center distance between the donor and the acceptor. ϵ_0 and ϵ_R refer to the vacuum permittivity and dielectric constant in the reaction. E_{ox} and E_{red} are the redox potentials estimated experimentally in *o*-DCB.

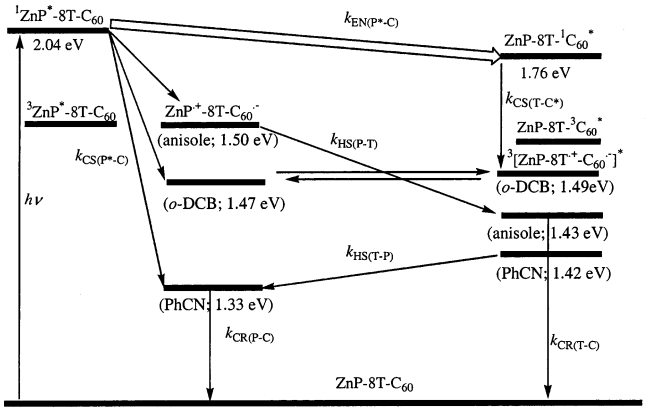

Figure 3. Schematic energy diagram and main processes for ZnP−8T−C_{60}; almost the same energy diagram was obtained for ZnP−4T−C_{60}.

as $k_d = (k_{IC} + k_{RAD} + k_{P*(ISC)})$, in which the rate constants refer to the internal conversion (IC), radiative (RAD), and intersystem crossing (ISC) processes of the ZnP moiety, respectively. In the case of ^{1}ZnP*−*n*T−C_{60}, the fluorescence intensity decreased while obeying almost a single-exponential function (> 95%); the shorter lifetime of ^{1}ZnP*−*n*T−C_{60} than that of ^{1}ZnP*−*n*T was estimated, as summarized in Table 3. Moreover, the τ_F values of ^{1}ZnP*−*n*T−C_{60} varied depending on the length of the *n*T moiety (Table 3).

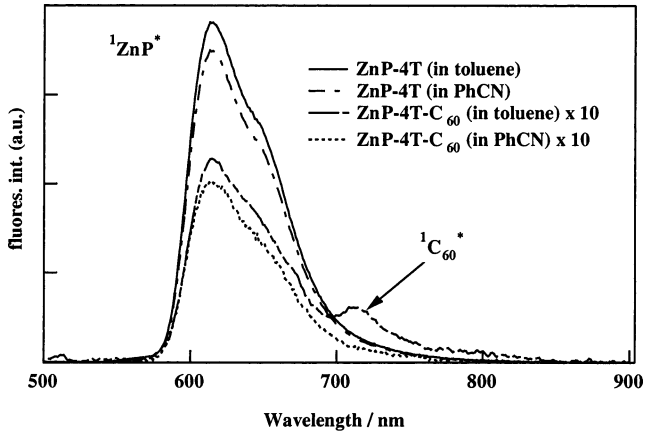

Figure 4. Fluorescence spectra of ZnP−8T and ZnP−8T−C_{60} in toluene and PhCN. Excitation wavelength 420 nm.

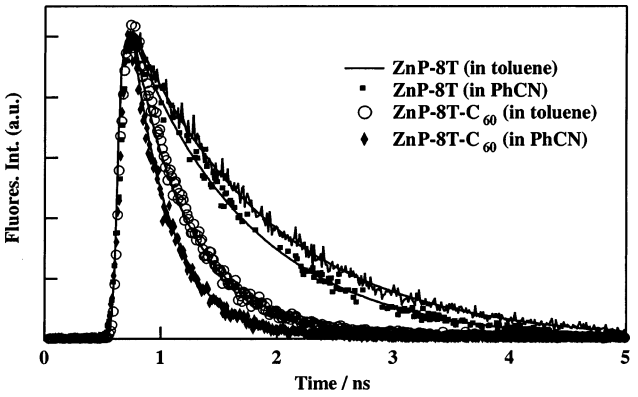

Figure 5. Fluorescence decay profiles around 650 nm of ZnP−8T and ZnP−8T−C_{60} in toluene and PhCN. Excitation wavelength 400 nm.

The rise of the fluorescence due to the $^1C_{60}$* moiety was confirmed around 710 nm in toluene, indicating the EN process from the ^{1}ZnP* moiety to the C_{60} moiety (eq 3), which is in good agreement with the appearance of the fluorescence of the $^1C_{60}$* moiety by the excitation of the ^{1}ZnP* moiety in the steady-state fluorescence spectra (Figure 4):

$$^1\text{ZnP}^*-n\text{T}-\text{C}_{60} \xrightarrow{k_{EN(P^*-C)}} \text{ZnP}-n\text{T}-{}^1\text{C}_{60}^* \qquad (3)$$

The CS process via ^{1}ZnP*−*n*T−C_{60} is impossible in toluene from the positive $\Delta G_{CS(P*-C)}$ values, which can be calculated from eq 2 using ΔG_{CR} in Table 2; therefore, this shortened τ_F

TABLE 3: Fluorescence Lifetimes (τ_F) of ^{1}ZnP* in Various Solvents

materials	toluene τ_F/ps	anisole τ_F/ps	*o*-DCB τ_F/ps	PhCN τ_F/ps
ZnP−4T	1200	1100	1000	1100
ZnP−4T−C_{60}[a]	50	40	40	40
ZnP−8T	1200	1100	920	980
ZnP−8T−C_{60}	460	400	300	330

[a] Estimation error of 5%.

TABLE 4: Rate Constants ($k_{EN(P^*-C)}$) and Quantum Yields ($\Phi_{EN(P^*-C)}$) for Energy Transfer from ^{1}ZnP*−*n*T−C_{60} to ZnP−*n*T−$^1C_{60}$*[a]

solvent	$k_{EN(P^*-C)}$ ($\Phi_{EN(P^*-C)}$)	$n = 4$	$n = 8$
	$k_{EN(P^*-C)}$[b]	1.9×10^{10}	1.3×10^9
toluene	$\Phi_{EN(P^*-C)}$[c]	0.95	0.61
anisole	$\Phi_{EN(P^*-C)}$[c]	0.76	0.52
o-DCB	$\Phi_{EN(P^*-C)}$[c]	0.76	0.39
PhCN	$\Phi_{EN(P^*-C)}$[c]	0.76	0.43

[a] The energy difference between ^{1}ZnP* and $^1C_{60}$* was evaluated to be 0.28 eV from the fluorescence bands. [b] The $k_{EN(P^*-C)}$ values were estimated from τ_F of ^{1}ZnP*−*n*T−C_{60} in toluene from eq 4. [c] The $\Phi_{EN(P^*-C)}$ values in toluene and in polar solvents were evaluated from eq 5, assuming that the k_{EN} values in polar solvents are the same as that in toluene.

value is due to the EN process from the ^{1}ZnP* moiety to the C_{60} moiety. The rate constant ($k_{EN(P^*-C)}$) and quantum yield ($\Phi_{EN(P^*-C)}$) for the EN process (eq 3) were estimated according to eqs 4 and 5 from the τ_0 and τ_F values of the triad ($\tau_{F,triad}$) in toluene.

$$k_{EN(P^*-C)} = (\tau_{F,triad})^{-1} - (\tau_0)^{-1} \quad (4)$$

$$\Phi_{EN(P^*-C)} = k_{EN(P^*-C)}/(\tau_{F,triad})^{-1} \quad (5)$$

Both the $k_{EN(P^*-C)}$ and $\Phi_{EN(P^*-C)}$ values drastically decreased from 1.9×10^{10} to 1.3×10^9 s^{-1} and from 0.95 to 0.61, respectively, by changing the *n*T moiety from 4T to 8T (Table 4). Thus, the *n*T moiety acts as the spacer for the EN process.

Fluorescence Lifetime Measurements in Polar Solvents. The k_{EN} values can be considered to be almost the same in solvents with similar refractive indices, which usually affects the k_{EN} values.[28] Thus, we assumed that the $k_{EN(P^*-C)}$ values are identical in the solvents employed in the present study. The $\Phi_{EN(P^*-C)}$ values were evaluated from eq 5 using the $\tau_{F,triad}$ values in polar solvents (Table 4).

The rate constant for the CS process between the ^{1}ZnP* and *n*T moieties in the triad ($k_{CS(P^*-T),triad}$) was evaluated by eq 6, assuming that $k_{CS(P^*-T),triad}$ is equal to that of the dyad ($k_{CS(P^*-T),dyad}$), because appreciable interaction is absent between the *n*T and C_{60} moieties, as suggested by the steady-state absorption spectra reported previously.[22a]

$$k_{CS(P^*-T),triad} = k_{CS(P^*-T),dyad} = (\tau_{F,dyad})^{-1} - \tau_0^{-1} \quad (6)$$

The $k_{CS(P^*-T),triad}$ values for ZnP−4T−C_{60} and ZnP−8T−C_{60} are $<10 \times 10^7$ s^{-1} and $(0.9-2.6) \times 10^8$ s^{-1}, respectively (Supporting Information Table S2).

Finally, the rate for the CS process from ^{1}ZnP* to C_{60} ($k_{CS(P^*-C)}$) can be evaluated from eq 7:

$$k_{CS(P^*-C)} = (\tau_{F,triad,polar\ solvent})^{-1} - (\tau_{F,triad,toluene})^{-1} - k_{CS(P^*-T),triad} \quad (7)$$

The $k_{CS(P^*-C)}$ value decreased from 5.0×10^9 to $(2.4-9.4) \times 10^8$ s^{-1} by changing from 4T to 8T, as listed in Table 5. The CS process generating distant CS states, ZnP$^{\bullet+}$−*n*T−$C_{60}^{\bullet-}$, via ^{1}ZnP*−*n*T−C_{60} has negative $\Delta G_{CS(P^*-C)}$ values in polar solvents. In this distant CS process, the *n*T moiety behaves like a molecular wire.[22a] For the processes (*X*) such as CS(P*−C) and CS(P*−T), the Φ_X values were evaluated by eq 8:

$$\Phi_X = k_X/[(\tau_{F,triad})^{-1}] \quad (8)$$

When k_x for the triad is set equal to $k_{CS(P^*-T),dyad}$ in eq 8, the quantum yields for ZnP$^{\bullet-}$−*n*T$^{\bullet+}$−C_{60} or ZnP$^{\bullet+}$−*n*T$^{\bullet-}$−C_{60} in the triad ($\Phi_{CS(P^*-T)}$) can be evaluated to be less than 0.08 (Supporting Information Table S2), suggesting that the contribution of such vicinal CS processes in the triads is quite small even in polar solvents. Possible CS processes of triads in polar solvents are shown in eqs 9 and 10:

$$^1\text{ZnP}^*\text{-}n\text{T-C}_{60} \xrightarrow{k_{CS(P^*\text{-}C)}\text{(moderate)}} \text{ZnP}^{+}\text{-}n\text{T-C}_{60}^{-} \quad (9)$$

$$^1\text{ZnP}^*\text{-}n\text{T-C}_{60} \xrightarrow{k_{CS(P^*\text{-}T),triad}\text{(minor)}} \text{ZnP}^{-}\text{-}n\text{T}^{+}\text{-C}_{60} + \text{ZnP}^{+}\text{-}n\text{T}^{-}\text{-C}_{60} \quad (10)$$

Transient Absorption Studies in PhCN. Figure 6a shows the picosecond transient absorption spectra of ZnP−8T−C_{60} in PhCN with the excitation of the ZnP moiety using a 560 nm laser light pulse. At 20 ps after the laser irradiation, the absorption bands of the ^{1}ZnP* moiety were confirmed around 520 and 580 nm with an absorption tail ranging to 1100 nm. Accompanying the decay of the ^{1}ZnP* absorption band, the absorptions appeared around 840 and 1050 nm, which are attributed to the 8T$^{\bullet+}$ moiety[16e,22,29] and the $C_{60}^{\bullet-}$ moiety, respectively.[30] Additionally, the absorption band of the ^{3}ZnP* moiety appeared at 780 nm, which was overlapped with the absorption band of the 8T$^{\bullet+}$ moiety. In Figure 6b, the temporal profile at 820 nm was curve-fitted by three components: the decay of ^{1}ZnP*−8T−C_{60}, the rise and decay of ^{3}ZnP*−8T−C_{60}, and the formation of ZnP−8T$^{\bullet+}$−$C_{60}^{\bullet-}$. The rate constant of the decay of the ^{1}ZnP* moiety, which can be considered to be the same as the rise of the ^{3}ZnP* moiety, was employed from the $(\tau_{F,triad})^{-1}$ value in PhCN (3.0×10^9 s^{-1}); thus, the time profile of 8T$^{\bullet+}$ was evaluated by subtracting these two lines from the observed time profile.

The slow generation rate of ZnP−8T$^{\bullet+}$−$C_{60}^{\bullet-}$ suggests the presence of some intermediate processes from ^{1}ZnP*−8T−C_{60} to ZnP−8T$^{\bullet+}$−$C_{60}^{\bullet-}$ (eq 11); for such processes, the energetically possible intermediate process is the EN process generating ZnP−8T−$^1C_{60}$* (eq 3) with $\Phi_{EN(P^*-C)} = 0.43$ in PhCN (Table 4). From the curve indicating the generation of ZnP−8T$^{\bullet+}$−$C_{60}^{\bullet-}$, the $k_{CS(T-C^*)}$ value was evaluated to be 1.3×10^8 s^{-1}.

$$\text{ZnP}-n\text{T}-{}^1\text{C}_{60}^* \xrightarrow{k_{CS(T-C^*)}} \text{ZnP}-n\text{T}^{\bullet+}-\text{C}_{60}^{\bullet-} \quad (11)$$

The vicinal CS(P*−T) process (eq 10) is thermodynamically possible; however, this process is ignorable because of low $\Phi_{CS(P^*-T)}$ (=0.06 (Supporting Information Table S2)).

In the case of ZnP−4T−C_{60}, the fast decay of the ^{1}ZnP* absorption band was also observed around 530 nm and the absorption band of the 4T$^{\bullet+}$ moiety appeared slowly around 700 nm.[16d,22a,28] This result implies that the generation process of ZnP−4T$^{\bullet+}$−$C_{60}^{\bullet-}$ is mainly attributed to eq 11 after the EN process from ^{1}ZnP*−4T−C_{60} to ZnP−4T−$^1C_{60}$* (eq 3).

Figure 7a shows the nanosecond transient absorption spectra of ZnP−8T−C_{60} in Ar-saturated PhCN after the nanosecond laser excitation at 560 nm. The characteristic transient absorption

TABLE 5: Driving Forces ($-\Delta G_{CS}$, $-\Delta G_{EN}$, and $-\Delta G_{HS}$) and Rate Constants ($k_{CS(P^*-C)}$, $k_{CS(T-C^*)}$, and $k_{HS(P-T)}$) of ZnP−*n*T−C_{60} in Anisole, *o*-DCB, and PhCN

				n = 4			*n* = 8		
solvent	initial state	final state		$-\Delta G^a$/eV	k/s^{-1}	Φ^b	$-\Delta G^a$/eV	k/s^{-1}	Φ^b
anisole	^{1}ZnP*−*n*T−C_{60}	ZnP$^{\bullet+}$−*n*T−$C_{60}^{\bullet-}$	$k_{CS(P^*-C)}$	0.56	5.0×10^9	0.20	0.54	2.4×10^8	0.11
	ZnP$^{\bullet+}$−*n*T−$C_{60}^{\bullet-}$	ZnP−*n*T$^{\bullet+}$−$C_{60}^{\bullet-}$	$k_{HS(P-T)}$	0.08	6.6×10^8		0.07	1.6×10^8	
	ZnP−*n*T−$^1C_{60}$*	ZnP−*n*T$^{\bullet+}$−$C_{60}^{\bullet-}$	$k_{CS(T-C^*)}$	0.36[c]			0.33[c]	2.4×10^9	0.16
o-DCB	^{1}ZnP*−*n*T−C_{60}	ZnP$^{\bullet+}$−*n*T−$C_{60}^{\bullet-}$	$k_{CS(P^*-C)}$	0.55	5.0×10^9	0.20	0.57	9.4×10^8	0.28
PhCN	^{1}ZnP*−*n*T−C_{60}	ZnP$^{\bullet+}$−*n*T−$C_{60}^{\bullet-}$	$k_{CS(P^*-C)}$	0.70	5.0×10^9	0.20	0.62	6.8×10^8	0.23
	ZnP−*n*T−$^1C_{60}$*	ZnP−*n*T$^{\bullet+}$−$C_{60}^{\bullet-}$	$k_{CS(T-C^*)}$	0.31[c]	4.0×10^9 [d]		0.34[c]	1.3×10^8 [d]	

[a] From eq 2 in the text and $-\Delta G_{HS(P-T)} = -\Delta G_{CR(T-C)} - (-\Delta G_{CR(P-C)})$. [b] From eq 8. [c] The ΔE_{0-0} value for $^1C_{60}$* is 1.76 eV in eq 2. [d] From eqs 15 and 16.

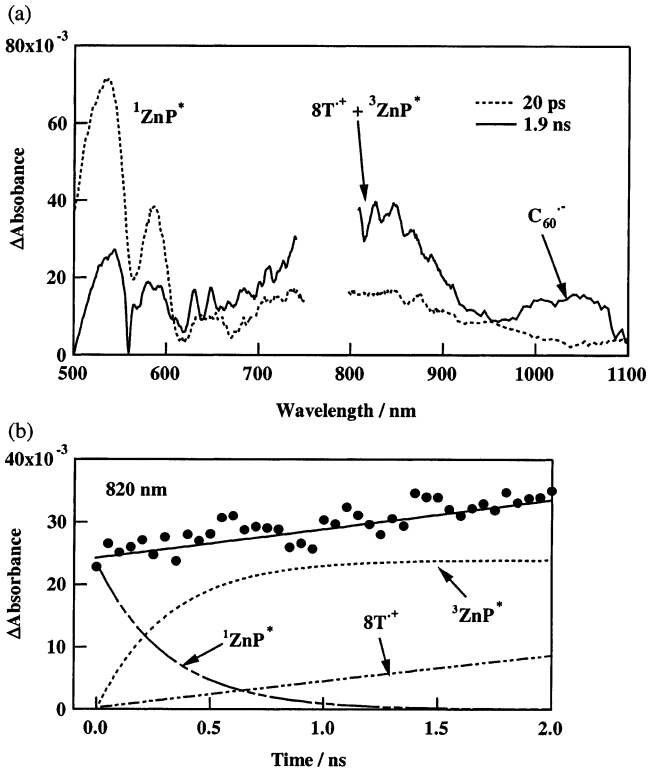

Figure 6. (a) Picosecond transient absorption spectra of ZnP−8T−C_{60} in PhCN (2.0×10^{-4} M) at 50 ps and 1.9 ns after 560 nm laser irradiation; (b) absorption time profiles at 820 nm.

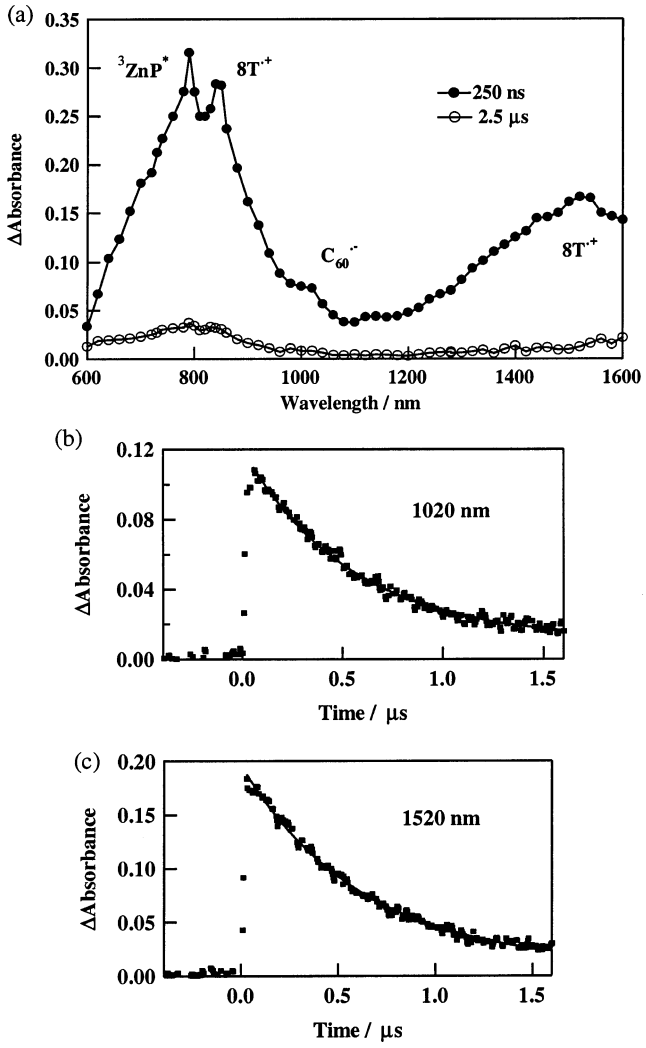

Figure 7. (a) Nanosecond transient absorption spectra of ZnP−8T−C_{60} (1.0×10^{-4} M) in PhCN at 250 ns (●) and 2.5 μs (○) after 560 nm laser irradiation; (b and c) absorption−time profiles at 1020 and 1520 nm, respectively.

bands of 8T$^{\bullet+}$ were observed at 840 nm and around 1520 nm[16e,22a] as well as the $C_{60}^{\bullet-}$ moiety at 1000 nm. Therefore, the CS state persisting in this time region was attributed to ZnP−8T$^{\bullet+}$−$C_{60}^{\bullet-}$. The absorption band around 700−800 nm was attributed to ^{3}ZnP*, indicating that ^{3}ZnP*−8T−C_{60} was also generated via an ISC process (Supporting Information Table S2 (k_d and Φ_d)). From the decay of the $C_{60}^{\bullet-}$ moiety (Figure 7b), the charge-recombination rate can be evaluated, which was equal to the rate for the absorption decay of 8T$^{\bullet+}$ at 1520 nm (Figure 7c). In the case of ZnP−4T−C_{60}, the transient absorption bands were observed at 700−780, 1000, and 1140 nm, which were attributed to ^{3}ZnP*, $C_{60}^{\bullet-}$, and 4T$^{\bullet+}$, respectively.[16d,22a]

The lifetimes of ZnP−*n*T$^{\bullet+}$−$C_{60}^{\bullet-}$ (τ_{RIP}) were evaluated to be 0.63 μs for *n*T = 4T and 0.83 μs for *n*T = 8T (Table 6), which were shorter than those of H_2P−*n*T$^{\bullet+}$−$C_{60}^{\bullet-}$ (2.4 μs for *n*T = 4T and 1.9 μs for *n*T = 8T).[22a] This difference in these τ_{RIP} values was due to the relation of the energy levels of Por−*n*T$^{\bullet+}$−$C_{60}^{\bullet-}$ and Por$^{\bullet+}$−*n*T−$C_{60}^{\bullet-}$. The energy of ZnP$^{\bullet+}$−*n*T−$C_{60}^{\bullet-}$ became lower than that of ZnP−*n*T$^{\bullet+}$−$C_{60}^{\bullet-}$ in PhCN (Table 2), while the energy of H_2P$^{\bullet+}$−*n*T−$C_{60}^{\bullet-}$ is higher than that of H_2P−*n*T$^{\bullet+}$−$C_{60}^{\bullet-}$. In the case of ZnP−*n*T−C_{60}, since the final CS state (ZnP$^{\bullet+}$−*n*T−$C_{60}^{\bullet-}$) was not confirmed in the transient absorption spectra, the CR process of ZnP$^{\bullet+}$−*n*T−$C_{60}^{\bullet-}$ was expected to occur as fast as the HS process from *n*T$^{\bullet+}$ to ZnP, as shown in eq 12, in which the CR process of ZnP$^{\bullet+}$−*n*T−$C_{60}^{\bullet-}$ may be even faster. Thus, the observed decay rates of ZnP−*n*T$^{\bullet+}$−$C_{60}^{\bullet-}$ are attributed to the apparent charge-recombination rates of ZnP−*n*T$^{\bullet+}$−$C_{60}^{\bullet-}$, which is the rate-determining step as listed in Table 6.

$$\text{ZnP}-n\text{T}^{\bullet+}-\text{C}_{60}^{\bullet-} \xrightarrow{k_{HS(T-P)}} \text{ZnP}^{\bullet+}-n\text{T}-\text{C}_{60}^{\bullet-} \xrightarrow{k_{CR(P-C)}} \text{ZnP}-n\text{T}-\text{C}_{60}$$

$$k_{CR(T-C)} \doteqdot k_{HS(T-P)} < k_{CR(P-C)} \qquad (12)$$

TABLE 6: Driving Forces ($-\Delta G_{CR}$ and $-\Delta G_{HS(P-T)}$) of the CR and HS Processes, Rate Constants (k_{CR}) for the CR Process, and Lifetimes of the Radical Ion Pair (τ_{RIP}) of ZnP−*n*T−C_{60} in Anisole, *o*-DCB, and PhCN

		n = 4				*n* = 8			
solvent	initial state[a]	$-\Delta G_{CR}$[b]/eV	$-\Delta G_{HS(P-T)}$[b]/eV	k_{CR}	τ_{RIP}/μs	$-\Delta G_{CR}$[b]/eV	$-\Delta G_{HS(P-T)}$[b]/eV	k_{CR}	τ_{RIP}/μs
Anisole	ZnP-nT$^{\bullet+}$-$C_{60}^{\bullet-}$	1.40	0.08	1.3×10^5 s^{-1}	7.7	1.43	0.07	1.1×10^5	9.1
o-DCB	ZnP-nT$^{\bullet+}$-$C_{60}^{\bullet-}$ ⇄ ZnP$^{\bullet+}$-nT-$C_{60}^{\bullet-}$	1.46 / 1.49	0.03	3.4×10^3 s^{-1},[c]	450	1.49 / 1.47	-0.02	1.1×10^3 s^{-1},[c]	910
PhCN	ZnP-nT$^{\bullet+}$-$C_{60}^{\bullet-}$	1.34	-0.11	1.6×10^6 s^{-1}	0.63	1.33	-0.09	1.2×10^6 s^{-1}	0.83

[a] The final CS state is ZnP−*n*T−C_{60}. [b] From eq 2 in the text and $-\Delta G_{HS(P-T)} = -\Delta G_{CR(T-C)} - (-\Delta G_{CR(P-C)})$. [c] At infinite dilution. Intermolecular CR rate constants at higher laser power: 8.5×10^9 M^{-1} s^{-1} for 4T and 1.1×10^9 M^{-1} s^{-1} for 8T.

In general, the singlet−triplet energy gap in the radical ion-pair state is characterized by the exchange interaction, which strongly depends on the distance between the two spins.[31] In ZnP$^{\bullet+}$−*n*T−$C_{60}^{\bullet-}$, they are separated by the *n*T moiety, which results in the small energy gap between the singlet and triplet spin states, mixing each other. Consequently, the lifetime of ZnP$^{\bullet+}$−*n*T−$C_{60}^{\bullet-}$ due to the charge recombination through the singlet spin state may be shorter than that of ZnP−*n*T$^{\bullet+}$−$C_{60}^{\bullet-}$ with the triplet spin state due to the relatively large exchange interaction.

Transient Absorption Studies in Anisole. When the ZnP moiety of ZnP−8T−C_{60} was excited with 560 nm laser light in anisole, the absorption bands were observed at 600−650 nm and at 1000−1100 nm, as shown in Figure 8a. The ZnP$^{\bullet+}$ moiety (600−650 nm)[32] showed the rise and decay (Figure 8b), while the absorption band of the $C_{60}^{\bullet-}$ moiety showed a monotonic rise, as shown in Figure 8c. This finding suggests that ZnP$^{\bullet+}$−8T−$C_{60}^{\bullet-}$ was directly produced from ^{1}ZnP*−8T−C_{60} (eq 9). Similarly, the direct generation of a remote CS state was also confirmed for ZnP−4T−C_{60}. As shown in Figure 8b, the temporal profile at 650 nm consists of three components, that is, two decay curves and one rise curve. When one of the decay curves is attributed to the ^{1}ZnP* moiety with the rate as evaluated from $(\tau_{F,triad})^{-1}$ being 2.5×10^9 s^{-1}, the deconvolution of the temporal profile gave the rising temporal profile of the ZnP$^{\bullet+}$ moiety at 650 nm with the rate constant, $k_{rise}(ZnP^{\bullet+}) = 2.3 \times 10^9$ s^{-1}. The $k_{CS(P^*-C)}$ values were evaluated from the rise of the ZnP$^{\bullet+}$ moiety by eq 13:

$$k_{CS(P^*-C)} = \Phi_{CS(P^*-C)} k_{rise}(ZnP^{\bullet+}) \qquad (13)$$

By substituting $\Phi_{CS(P^*-C)} = 0.11$ (Table 5), the rate constant ($k_{CS(P^*-C)}$) for the generation of the ZnP$^{\bullet+}$ moiety from the ^{1}ZnP* moiety was evaluated to be 2.5×10^8 s^{-1}. Moreover, the decay rate of the ZnP$^{\bullet+}$ moiety gave the rate constant ($k_{HS(P-T)}$) for the HS process from ZnP$^{\bullet+}$ to 8T (eq 14), which was evaluated to be 1.6×10^8 s^{-1}. The *n*T moiety acted as a cation trapper from the ZnP$^{\bullet+}$ moiety similar to H_2P−*n*T$^{\bullet+}$−$C_{60}^{\bullet-}$.[22a]

$$ZnP^{\bullet+}-nT-C_{60}^{\bullet-} \xrightarrow{k_{HS(P-T)}} ZnP-nT^{\bullet+}-C_{60}^{\bullet-} \qquad (14)$$

In Figure 8c, the temporal profile at 1030 nm consists of three components, that is, one decay curve and two rise curves. The decay profile is attributed to the absorption tail of the ^{1}ZnP* moiety, while the rise components are due to the $C_{60}^{\bullet-}$ and $^1C_{60}$* moieties. The $C_{60}^{\bullet-}$ moiety was formed directly and indirectly; the former is the direct CS process via ^{1}ZnP*−*n*T−C_{60} (eq 9)

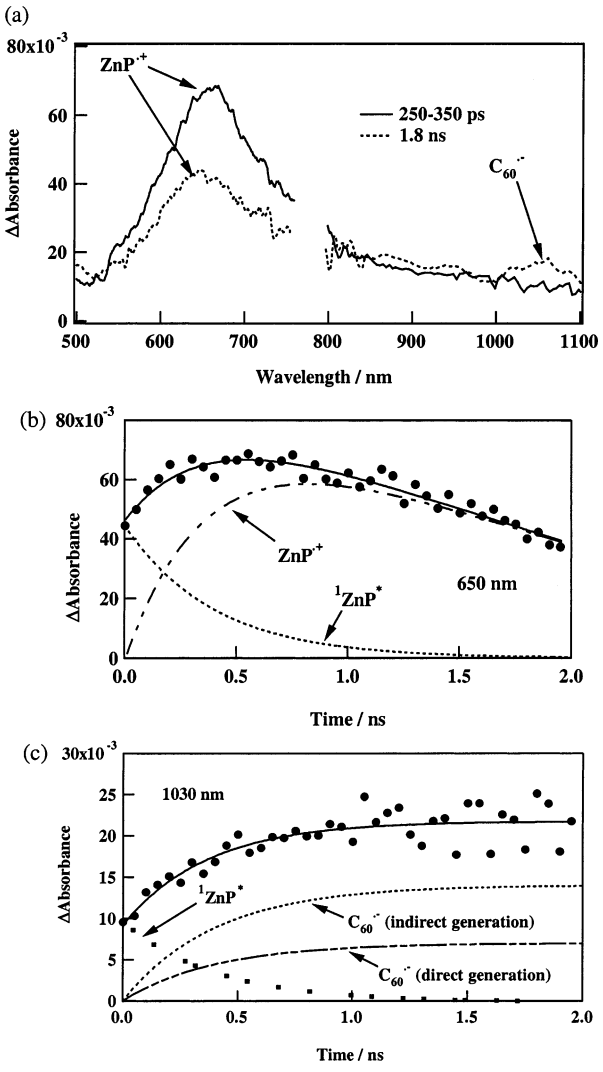

Figure 8. (a) Picosecond transient absorption spectra of ZnP−8T−C_{60} in anisole (2.0×10^{-4} M) at 250−350 ps and 1.8 ns after 560 nm laser irradiation; (b and c) absorption−time profiles at 650 and 1030 nm, respectively.

which is almost the same rate as the rise of the ZnP$^{\bullet+}$ moiety ($k_{direct}(C_{60}^{\bullet-})$ in Figure 8c), while the latter is the CS process via ZnP−*n*T−$^1C_{60}$* ($k_{indirect}(C_{60}^{\bullet-})$) which was calculated by subtraction of the superposition of the decay of ^{1}ZnP* and the direct generation from the best-fitted curve, giving an apparent rate of 3.2×10^9 s^{-1}. Direct observation of the rise and decay of the $^1C_{60}$* moiety was difficult, because of its broad absorption

in the 900−1000 nm region, with which the absorption tails of ^{1}ZnP* and $C_{60}^{\bullet-}$ were overlapped. Furthermore, the $k_{indirect}(C_{60}^{\bullet-})$ value was larger than the rate for the generation of the $^1C_{60}$* moiety (1.3×10^9 s^{-1}): $k_{indirect}(C_{60}^{\bullet-}) > k_{EN(P^*-C)}$. However, taking the fluorescence lifetime of $NMPC_{60}$ (1.30 ns) into consideration, the values of $k_{CS(T-C^*)}$ (2.4×10^9 s^{-1}) and $\Phi_{CS(T-C^*)}$ (0.16) were calculated using eqs 15 and 16.

$$k_{CS(T-C^*)} = k_{obs}(C_{60}^{\bullet-}) - \tau_F(NMPC_{60})^{-1} \quad (15)$$

$$\Phi_{CS(T-C^*)} = \Phi_{ET(P^*-C)}[k_{CS(T-C^*)}/k_{indirect}(C_{60}^{\bullet-})] \quad (16)$$

Comparing the absorption temporal profile at 650 nm with that at 1030 nm, the absorption of the $C_{60}^{\bullet-}$ moiety remains after 0.5 ns, while the $ZnP^{\bullet+}$ moiety begins to decay. This finding supports that the HS process occurs from the $ZnP^{\bullet+}$ moiety to the 8T moiety (eq 14).

In the case of ZnP−4T−C_{60}, the analysis of the absorption temporal profile at 1000 nm was difficult, because the absorption bands of the $^1C_{60}$* and ^{1}ZnP* moieties were overlapped with that of the $C_{60}^{\bullet-}$ moiety.

In the microsecond region, the absorption bands due to the $C_{60}^{\bullet-}$, $8T^{\bullet+}$, and ^{3}ZnP* moieties were confirmed, indicating the generation of ZnP−$8T^{\bullet+}$−$C_{60}^{\bullet-}$ and ^{3}ZnP*−8T−C_{60}. The $k_{CR(T-C)}$ value was evaluated, as listed in Table 6, from which the τ_{RIP} values were estimated to be 7.7 and 9.1 μs for ZnP−$4T^{\bullet+}$−$C_{60}^{\bullet-}$ and ZnP−$8T^{\bullet+}$−$C_{60}^{\bullet-}$, respectively, which were almost the same as those of H_2P−$nT^{\bullet+}$−$C_{60}^{\bullet-}$ (5.3 μs for nT = 4T and 4.5 μs for nT = 8T, Supporting Information Table S3). Since ZnP−$nT^{\bullet+}$−$C_{60}^{\bullet-}$ is more stable than $ZnP^{\bullet+}$−nT−$C_{60}^{\bullet-}$ in anisole (Table 2), it is indicated that the final CR process takes place via ZnP−$nT^{\bullet+}$−$C_{60}^{\bullet-}$ to the neutral triads (eq 17) similar to that of H_2P−$nT^{\bullet+}$−$C_{60}^{\bullet-}$.[22a]

$$ZnP-nT^{\bullet+}-C_{60}^{\bullet-} \xrightarrow{k_{CR(T-C)}} ZnP-nT-C_{60} \quad (17)$$

Transient Absorption Studies in *o*-DCB. In *o*-DCB, the picosecond transient absorption spectra were not obtained, because the ZnP moiety was degraded seriously by the intense femtosecond laser in solvents including halogen atoms. On the other hand, the nanosecond transient absorption spectra in *o*-DCB were observed without degradation of the ZnP moiety, because of the low laser power of the nanosecond laser pulse.

Figure 9a shows the nanosecond transient absorption spectra of ZnP−8T−C_{60} observed at 50 μs in Ar- and O_2-saturated *o*-DCB. In the Ar-saturated solution, the absorption bands of the $ZnP^{\bullet+}$, $8T^{\bullet+}$, $C_{60}^{\bullet-}$, and ^{3}ZnP* moieties were confirmed. In O_2-saturated *o*-DCB, the absorption bands of the ^{3}ZnP* moiety vanished, while the long-lived $ZnP^{\bullet+}$, $8T^{\bullet+}$, and $C_{60}^{\bullet-}$ moieties remained, as seen in Figure 9a. Thus, the kinetic analysis can be performed without interference of the huge absorption bands of the ^{3}ZnP* moiety. The absorption band attributed to the $8T^{\bullet+}$ moiety (>1300 nm) becomes broad with a red shift compared with that in PhCN; similarly, a red shift was confirmed in the $ZnP^{\bullet+}$ moiety (680 nm), where $ZnTPP^{\bullet+}$ appeared around 620 nm.[32]

In O_2-saturated *o*-DCB, initial decays of the absorption bands $ZnP^{\bullet+}$, $8T^{\bullet+}$, and C_{60} seem to be faster than those in Ar-saturated solution; the slow decay component of the $8T^{\bullet+}$ moiety remains over 2−3 ms in both Ar-saturated and O_2-saturated *o*-DCB, as shown in Figure 9b. It is notable that the $ZnP^{\bullet+}$, $8T^{\bullet+}$, and $C_{60}^{\bullet-}$ moieties decayed at the same rate. Thus, it was concluded that ZnP−$nT^{\bullet+}$−$C_{60}^{\bullet-}$ and $ZnP^{\bullet+}$−nT−$C_{60}^{\bullet-}$ were present as an equilibrium mixture in the singlet spin state, as shown by eq

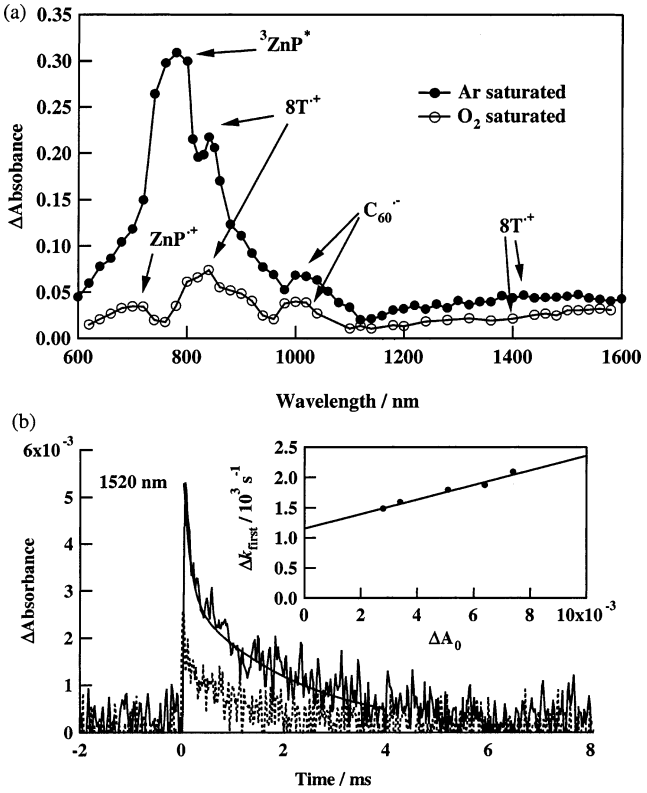

Figure 9. (a) Nanosecond transient absorption spectra of ZnP−8T−C_{60} (1.0×10^{-4} M) in *o*-DCB at 50 μs in Ar-saturated (●) and O_2-saturated (○) after 560 nm laser irradiation; (b) absorption−time profiles at 1520 nm. Inset: laser-power dependence of the CR rate.

18. This was supported by the similarity of the energy of ZnP−$nT^{\bullet+}$−$C_{60}^{\bullet-}$ to that of $ZnP^{\bullet+}$−nT−$C_{60}^{\bullet-}$.

$$[ZnP-nT^{\bullet+}-C_{60}^{\bullet-} \rightleftarrows ZnP^{\bullet+}-nT-C_{60}^{\bullet-}] \xrightarrow{k_{CR}} ZnP-nT-C_{60} \quad (18)$$

The temporal profile of the $8T^{\bullet+}$ moiety in Ar-saturated *o*-DCB showed two step-decays: the intramolecular CR (CR^{intra}) process and the intermolecular back electron-transfer (BET^{inter}) process (eq 19). The apparent decay rate strongly depended on the laser power, which varies the concentration of the radical ions.

$$(ZnP-nT)^{\bullet+}-C_{60}^{\bullet-} + (ZnP-nT)^{\bullet+}-C_{60}^{\bullet-} \xrightarrow{k_{BET}^{inter}} ZnP-nT-C_{60} + ZnP-nT-C_{60} \quad (19)$$

Hence, the rate constants were estimated from the decay of the $nT^{\bullet+}$ moiety by eq 20.

$$-d[\ln(\Delta A_0)]/dt = \Delta k_{first} = k_{CR}^{intra} + (2k_{BET}^{inter}/\epsilon_{nT})\Delta A_0 \quad (20)$$

Hereby, ΔA_0 refers to the absorbance at $t = 0$, k_{first} refers to the first-order rate constant evaluated in the initial part of the decay, k_{CR}^{intra} and k_{BET}^{inter} refer to the rate constants for the intramolecular CR process between the $C_{60}^{\bullet-}$ and $nT^{\bullet+}$/$ZnP^{\bullet+}$ moieties and intermolecular back electron transfer, respectively, and ϵ_{nT} refers to an extinction coefficient of the absorption band of $nT^{\bullet+}$.[22] From the laser-power dependence of the ΔA_0 and k_{first} values, a linear relation between the k_{first} and ΔA_0 values was obtained, as shown in the inset of Figure 9b. From the intercept, the k_{CR}^{intra} value was estimated to be 1.1×10^3 s^{-1}, which corresponds to $\tau_{RIP} = 910$ μs. From the slope and ϵ_{nT}, the k_{BET}^{inter} value was estimated to be 1.1×10^9 M^{-1} s^{-1} for ZnP−

8T−C_{60} in *o*-DCB. The intermolecular BET process takes place near the diffusion-controlled limit ($k_{diff} = 5.0 \times 10^9$ M^{-1} s^{-1} in *o*-DCB).[28]

Comparison with $H_2P-nT-C_{60}$. In the case of ZnP−*n*T−C_{60}, the final CS states depended on the solvent polarity, while the final CS state for $H_2P-nT-C_{60}$ was $H_2P-nT^{\bullet+}-C_{60}^{\bullet-}$ independent of the solvent property. In *o*-DCB, the τ_{RIP} values for $ZnP-nT^{\bullet+}-C_{60}^{\bullet-}$ (450−910 μs) were extremely longer than those for $H_2P-nT^{\bullet+}-C_{60}^{\bullet-}$ (14−27 μs). Considering the relation of the energy levels of the CS states ($\Delta G_{RIP}(ZnP-nT^{\bullet+}-C_{60}^{\bullet-}) = \Delta G_{RIP}(ZnP^{\bullet+}-nT-C_{60}^{\bullet-})$ and $\Delta G_{RIP}(H_2P-nT^{\bullet+}-C_{60}^{\bullet-}) < \Delta G_{RIP}(H_2P^{\bullet+}-nT-C_{60}^{\bullet-})$), this difference in the τ_{RIP} values is due to the equilibrium of $ZnP-nT^{\bullet+}-C_{60}^{\bullet-}$ and $ZnP^{\bullet+}-nT-C_{60}^{\bullet-}$, as described in eq 18.

In anisole, the τ_{RIP} values of $ZnP-nT^{\bullet+}-C_{60}^{\bullet-}$ (7.7−9.1 μs) are almost the same values as those of $H_2P-nT^{\bullet+}-C_{60}^{\bullet-}$ (5.3−4.5 μs), since $\Delta G_{RIP}(ZnP-nT^{\bullet+}-C_{60}^{\bullet-}) < \Delta G_{RIP}(ZnP^{\bullet+}-nT-C_{60}^{\bullet-})$ is the same tendency with the ΔG_{RIP} values for $H_2P-nT-C_{60}$. The final CR process via $ZnP-nT^{\bullet+}-C_{60}^{\bullet-}$ may be relatively slow because of the Marcus inverted region similar to that of $H_2P-nT^{\bullet+}-C_{60}^{\bullet-}$.[22a] Furthermore, the triplet spin character of this vicinal radical ion pair may also prolong the lifetimes.[31]

In PhCN, on the other hand, the τ_{RIP} values of $ZnP-nT^{\bullet+}-C_{60}^{\bullet-}$ (0.63−0.83 μs) were shorter than those of $H_2P-nT^{\bullet+}-C_{60}^{\bullet-}$ (1.9−2.4 μs), indicating that the CR process may occur via $ZnP^{\bullet+}-nT-C_{60}^{\bullet-}$ with a short lifetime, while the CR process occurs via $H_2P-nT^{\bullet+}-C_{60}^{\bullet-}$ with a longer lifetime.

Conclusion

The charge separation of ZnP−*n*T−C_{60} by excitation of the ^{1}ZnP* moiety gave two CS sates; one is $ZnP^{\bullet+}-nT-C_{60}^{\bullet-}$ generated by the direct CS process via ^{1}ZnP* with a wirelike performance of the *n*T moiety, and the other is CS $ZnP-nT^{\bullet+}-C_{60}^{\bullet-}$ generated by the indirect CS process via $^1C_{60}$* after the EN process from ^{1}ZnP* to C_{60}. $ZnP-nT^{\bullet+}-C_{60}^{\bullet-}$ was also generated by the HS process from $ZnP^{\bullet+}-nT-C_{60}^{\bullet-}$. The electron-transfer processes were successfully controlled by the solvent polarity. In the case of *o*-DCB, the τ_{RIP} values were estimated to be extremely long compared with those in the other solvents and $H_2P-nT^{\bullet+}-C_{60}^{\bullet-}$ in *o*-DCB. These long τ_{RIP} values may be caused by the equilibrium between $ZnP-nT^{\bullet+}-C_{60}^{\bullet-}$ and $ZnP^{\bullet+}-nT-C_{60}^{\bullet-}$ with similar energies in *o*-DCB. The roles of the *n*T moieties vary much with the length, electronic factors, and medium effects.

Acknowledgment. The present work was partly supported by a Grant-in-Aid for Scientific Research on Priority Area (417) from the Ministry of Education, Science, Sports and Culture of Japan.

Supporting Information Available: Optimized structures and the HOMO and LUMO. Tables for free-energy changes for charge separation and charge recombination. Table for rate constants and quantum yields. Calculation of energy-transfer rate constants. Charge-recombination data of $H_2P-nT-C_{60}$ in anisole. This material is available free of charge via the Internet at http://pubs.acs.org.

References and Notes

(1) Winkler, J. R.; Gray, H. B. *Chem. Rev.* **1992**, *92*, 369.

(2) Langen, R.; Chang, I. J.; Germanas, J. P.; Richards, J. H.; Winkler, J. R.; Gray, H. B. *Science* **1995**, *268*, 1733.

(3) (a) Imahori, H.; Sakata, Y. *Eur. J. Org. Chem.* **1999**, 2445. (b) Imahori, H.; Sakata Y. *Adv. Mater.* **1997**, *9*, 537.

(4) (a) Davis, W. B.; Ratner, M. A.; Wasielewski, M. R. *Chem. Phys.* **2002**, *281*, 333. (b) Miller, S. E.; Lukas, A. S.; Marsh, E.; Bushard, P.; Wasielewski, M. R. *J. Am. Chem. Soc.* **2000**, *122*, 7802. (c) Gosztola, D.; Wang, B.; Wasielewski, M. R. *J. Photochem. Photobiol., A* **1996**, *102*, 71. (d) Wasielewski, M. R. *Chem. Rev.* **1992**, *92*, 395.

(5) Verhoeven, J. W.; Scherer, T.; Willemse, R. J. *Pure Appl. Chem.* **1993**, *65*, 1717.

(6) Guldi, D. M.; Asmus, K. D. *J. Am. Chem Soc.* **1997**, *119*, 5744.

(7) Verhoeven, J. W. *Pure Appl. Chem.* **1990**, *62*, 1585.

(8) Page, C. C.; Moser, C. C.; Chen, X.; Dutton, P. L. *Nature* **1999**, *402*, 47.

(9) (a) Luo, C.; Guldi, D. M.; Imahori, H.; Tamaki, K.; Sakata, Y. *J. Am. Chem. Soc.* **2000**, *122*, 6535. (b) Fukuzumi, S.; Imahori, H.; Yamada, H.; El-Khouly, M. E.; Fujitsuka, M.; Ito, O.; Guldi, D. M. *J. Am. Chem. Soc.* **2001**, *123*, 2571. (c) Imahori, H.; Tamaki, K.; Guldi, D. M.; Luo. C.; Fujitsuka, M.; Ito, O.; Fukuzumi, S. *J. Am. Chem. Soc.* **2001**, *123*, 2607. (d) Imahori, H.; Guldi, D. M.; Tamaki, K.; Yoshida, Y.; Luo, C.; Sakata, Y.; Fukuzumi, S. *J. Am. Chem. Soc.* **2001**, *123*, 6617. (e) Imahori, H.; Tamaki, K.; Araki, Y.; Sekiguchi, Y.; Ito, O.; Sakata, Y.; Fukuzumi, S. *J. Am. Chem. Soc.* **2002**, *124*, 5165.

(10) Lindell, P. A.; Kuciauskas, D.; Sumida, J. P.; Nash, B.; Nguyen, D.; Moore, A. L.; Moore, T. A.; Gust, D. *J. Am. Chem. Soc.* **1997**, *119*, 1400. (b) Carbonera, D.; Di Valentin, M.; Corvaja, C.; Agostini, G.; Giacometti, G.; Liddell, P. A.; Kuciauskas, D.; Moore, A. L.; Moore, T. A.; Gust, D. *J. Am. Chem. Soc.* **1998**, *120*, 4398.

(11) (a) Marcus, R. A. *J. Chem. Phys.* **1956**, *24*, 966. (b) Marcus, R. A. *J. Chem. Phys.* **1957**, *26*, 867. (c) Marcus, R. A. *J. Chem. Phys.* **1957**, *26*, 872. (d) Marcus, R. A. *J. Chem. Phys.* **1965**, *43*, 679. (e) Marcus, R. A.; Sutin, N. *Biochim. Biophys. Acta* **1985**, *811*, 265.

(12) Kroto, H. W.; Heath, J. R.; O'Brien, S, C.; Curl, R. F.; Smalley, R. E. *Nature* **1985**, *318*, 162. (b) Sogoshi, N., Kato, Y.; Wakabayashi, T.; Momose, T.; Tam, S.; DeRose, M. E.; Fajardo, M. E. *J. Phys. Chem. A* **2000**, *104*, 3733.

(13) (a) Haddon, R. C. *Acc. Chem. Res.* **1988**, *21*, 243. (b) Haddon, R. C. *Science* **1993**, *261*, 1545.

(14) (a) Maggini, M.; Scorrano, G.; Prato, M. *J. Am. Chem. Soc.* **1993**, *115*, 9798. (b) Guldi, D. M.; Prato, M. *Acc. Chem. Res.* **2000**, *33*, 695.

(15) (a) Allemand, P. H.; Koch, A.; Wudl, F.; Rubin, F.; Y.; Diederich, F.; Alvarenz, M. M.; Anz, S. J.; Whetten, R. L. *J. Am. Chem. Soc.* **1991**, *113*, 1050. (b) Dubois, D.; Kadish, K. M.; Flanagan, S.; Haufler, R. E.; Chibante, L. P. F.; Wilson, L. J. *J. Am. Chem. Soc.* **1991**, *113*, 4364.

(16) (a) D'Souza, F.; Deviprasad, G. R.; Zandler, M. E.; El-Khouly, M. E.; Fujitsuka, M.; Ito, O. *J. Phys. Chem. A* **2003**, *107*, 4801. (b) D'Souza, F.; Zandler, M. E.; Smith, P. M.; Deviprasad, G. R.; Arkady, K.; Fujitsuka, M.; Ito, O. *J. Phys. Chem. A* **2002**, *106*, 649. (c) D'Souza, F.; Deviprasad, G. R.; Zandler, M. E.; El-Khouly, M E.; Fujitsuka, M.; Ito, O. *J. Phys. Chem. B.* **2002**, *106*, 4952. (d) Fujitsuka, M.; Matsumoto, K.; Ito, O.; Yamashiro, T.; Aso, Y.; Otsubo, T. *Res. Chem. Intermed.* **2001**, *27*, 73. (e) Fujitsuka, M.; Ito, O.; Yamashiro, T.; Aso, Y.; Otsubo, T. *J. Phys. Chem. A* **2000**, *104*, 4876. (f) Tkachenko, N. V.; Rantala, L.; Tauber, A. Y.; Helaja, J.; Hynninen, P. V.; Lemmetyinen, H. *J. Am. Chem. Soc.* **1999**, *121*, 9378. (g) Schuster, D. I.; Cheng, P.; Wilson, S. R.; Prokhorenko, V.; Katterle, M.; Holzwarth, A. R.; Braslavsky, S. E.; Klihm, G.; Williams, R. M.; Luo, C. *J. Am. Chem. Soc.* **1999**, *121*, 11599. (h) Guldi, D. M.; Garscia, G. T.; Mattay, J. *J. Phys. Chem. A* **1998**, *102*, 9679. (i) Guldi, D. M.; Maggini, M.; Scorrano, G.; Prato, M. *J. Am. Chem. Soc.* **1997**, *119*, 974. (j) Bell, T. D. M.; Smith, T. A.; Ghiggino, K. P.; Ranasinghe, M. G.; Shephard, M. J.; Paddon-Row: M. N. *Chem. Phys. Lett.* **1997**, *268*, 223. (k) Imahori, H.; Hagiwara, K.; Akiyama, T.; Aoki, M.; Taniguchi, S.; Okada, T.; Shirakawa, M.; Sakata, Y. *Chem. Phys. Lett.* **1996**, *263*, 545. (l) Williams, R. M.; Zwier, M. N.; Verhoeven, J. W. *J Am. Chem. Soc.* **1995**, *117*, 4093. (m) Imahori, H.; Cardoso, S.; Tatman, D.; Lin, S.; Noss, L.; Seely, G. R.; Sereno, L.; Silber, C.; Moore, T. A.; Moore, A. L.; Gust, D. *J. Photochem. Photobiol., A* **1995**, *62*, 1009.

(17) (a) Smirnov, S. N.; Liddell, P. A.; Vlassiouk, I. V.; Teslja, A.; Kuciauskas, D.; Braun, C. L.; Moore, A. L.; Moore, T. A.; Gust, D. *J. Phys. Chem. A* **2003**, *107*, 7567. (b) Kodis, G.; Liddell, P. A.; de la Garza, L.; Moore, A. L.; Moore, T. A.; Gust, D. *J. Mater. Chem.* **2002**, *12*, 2100. (c) Carbonera, D.; Di Valentin, M.; Corvaja, C. Agostini, G.; Giacometti, G.; Liddell, P. A.; Kuciauskas, D.; Moore, A. L.; Moore, T. A.; Gust, D. *J. Am. Chem. Soc.* **1998**, *120*, 4398. (d) Gust, D.; Moore, T. A.; Moore, A. L.; Macpherson, A. N.; Lopez, A.; DeGraziano, J. M.; Gouni, I.; Bittersmann, E.; Seely, G. R.; Gao, F.; Nieman, R. A.; Ma, X. C.; Demanche, L.; Luttrull, D. K.; Lee, S.-J.; Kerrigan, P. K. *J. Am. Chem. Soc.* **1993**, *115*, 11141. (e) Gust, D.; Moore, T. A.; Moore, A. L.; Lee, S.-J.; Bittersmann, E.; Luttrull, D. K.; Rehms, A. A.; De Graziano, J. M.; Ma, X. C.; Gao, F.; Belford, R. E.; Trier, T. T. *Science* **1990**, *248*, 199.

(18) Ramos, A. M.; Meskers, S. C. J.; van Hal, P. A.; Knol, J.; Hummelen, J. C.; Janssen, R. A. J. *J. Phys. Chem. A* **2003**, *107*, 9269.

(19) Sanchez, L.; Perez, I.; Martin, N.; Guldi, D. M. *Chem.—Eur. J.* **2003**, *9*, 2457.

(20) D'Souza, F.; Zandler, M. E.; Smith, P. M.; Deviprasad, G. R.; Arkady, K. Fujitsuka, M.; Ito, O. *J. Phys. Chem. A* **2002**, *106*, 649.

(21) Greenfield, S. R.; Svec, W. A.; Gosztola, D.; Wasielewski, M. R. *J. Am. Chem. Soc.* **1996**, *118*, 6767.

(22) (a) Nakamura, T.; Fujitsuka, M.; Araki, Y.; Ito, O.; Ikemoto, J.; Takimiya, K.; Aso,Y.; Otsubo, T. *J. Phys. Chem. B* **2004**, *108*, 10700. (b) Ikemoto, J.; Takimiya, K.; Aso, Y.; Fujitsuka, M.; Ito, O. *Org. Lett.* **2002**, **4**, 309. (c) Otsubo, T.; Aso, Y.; Takimiya, K. *J. Mater. Chem.* **2002**, *12*, 2565. (e) Otsubo, T.; Aso, Y.; Takimiya, K. *Bull. Chem. Soc. Jpn.* **2001**, *74*, 1789.

(23) Lukas, A. S.; Zhao, Y.; Miller, S. E.; Wasielewski, M. R. *J. Phys. Chem. B* **2002**, *106*, 1299.

(24) Weller, A. *Z. Phys. Chem.* **1982**, *132*, 93.

(25) (a) Brocks, G. *Synth. Met.* **1999**, *102*, 914. (b) Moro, G.; Scalmani, G.; Cosentio, U.; Pitea, D. *Synth. Met.* **1998**, *98*, 69. (c) Moro, G.; Scalmani, G.; Cosentio, U.; Pitea, D. *Synth. Met.* **2000**, *108*, 165. (d) Telesca, R.; Bolink, H.; Yunoki, S.; Hadziioannou, G.; Van Doijnnen, P. Th.; Snijders, J. G.; Jonkman, H. T.; Sawatzky, G. A. *Phys. Rev. B* **2001**, *63*, 155112. (e) Geskin, V. M.; Dkhissi, A.; Brèdas, J. L. *Int. J. Quantum Chem.* **2003**, *91*, 350.

(26) Frisch, M. J.; Trucks, G. W.; Schlegel, H. B.; Scuseria, G. E.; Robb, M. A.; Cheeseman, J. R.; Zakrzewski, V. G.; Montgomery, J. A., Jr.; Stratmann, R. E.; Burant, J. C.; Dapprich, S.; Millam, J. M.; Daniels, A. D.; Kudin, K. N.; Strain, M. C.; Farkas, O.; Tomasi, J.; Barone, V.; Cossi, M.; Cammi, R.; Munnucci, B.; Pomelli, C.; Adamo, C.; Clifford, S.; Ochterski, J.; Petersson, G. A.; Ayala, P. Y.; Cui, Q.; Morokuma, K.; Malick, D. K.; Rabuck, A. D.; Raghavachari, K.; Foresman, J. B.; Cioslowski, J.; Oritz, J. V.; Baboul, A. G.; Stefanov, B. B.; Liu, G.; Liashenko, A.; Piskorz, P.; Komaromi, I.; Gomperts, R.; Martin, R. L.; Fox, D. J.; Keith, T.; Al-Laham, M. A.; Peng, C. Y.; Nnayakkara, A.; Gonzalez, C.; Challacombe, M.; Gill, P. M. W.; Johnson, B. Chen, W.; Wong, M. W.; Andres, J. L.; Gonzalez, C.; Head-Gordon, M.; Replogle, E. S.; Popel, J. A. *Gaussian 98*, revision A.7; Gaussian, Inc.: Pittsburgh, PA, 1998.

(27) Murov, S. L.; Carmichael, I.; Hug, G. L. *Handbook of Photochemistry*; Marcel Dekker: NewYork, 1993; p 207.

(28) (a) Förster, T. *Natuwissenschaften* **1946**, *33*, 166−175. (b) Förster, T. *Ann. Phys.* **1948**, *2*, 55. (c) Calvert, J. G.; Pitts, J. N., Jr. *Photochemistry*; John Wiley & Sons: New York, 1967; pp 339−365.

(29) (a) Becker, R. S.; de Melo, J. S.; Maçanita, A. L.; Elisei, F. *J. Phys. Chem.* **1996**, *100*, 18683. (b) Becker, R. S.; de Melo, J. S.; Maçanita, A. L.; Elisei, F. *Pure Appl. Chem.* **1995**, *67*, 9.

(30) Matsumoto, K.; Fujitsuka, M.; Sato, T.; Onodera, S.; Ito, O. *J. Phys. Chem. B* **2000**, *104*, 11632.

(31) (a) Wegner, M.; Fisher, H.; Koeberg, M.; Verhoeven, J. W.; Oliver, A. M.; Paddom-Row: M. N. *Chem. Phys*. **1999**, *242*, 227. (b) Hviid, L.; Bouwman, W. G.; Paddom-Row: M. N.; van Ramesdonk, H. J.; Verhoeven, J. W.; Brouwer, A. M. *Photochem. Photobiol. Sci*. **2003**, *2*, 995. (c) Hviid, L.; Verhoeven, J. W.; Brouwer, A. M.; Paddom-Row, M. N.; Yang, J. *Photochem. Photobiol. Sci.* **2004**, *3*, 246.

(32) (a) Chosrowjan, H.; Taniguchi, S.; Okada, T.; Takagi, S.; Arai, T.; Tokunaga, K. *Chem. Phys. Lett.* **1995**, *242*, 644. (b) Fajer, J.; Borg, D. C.; Forman, A.; Dolpin, D.; Felton, R. H. *J. Am. Chem. Soc.* **1970**, *92*, 3451.